2010

Minority carrier lifetime variations associated with misfit dislocation networks in heteroepitaxial GaInP

Haegel, Nancy M.

Semicond. Sci. Technol. **25** (2010) 055017 (6pp) doi:10.1088/0268-1242/25/5/055017

Minority carrier lifetime variations associated with misfit dislocation networks in heteroepitaxial GaInP

Nancy M Haegel[1], **Scott E Williams**[1], **C L Frenzen**[2] **and Clyde Scandrett**[2]

[1] Physics Department, Naval Postgraduate School, Monterey, CA 93943, USA
[2] Applied Mathematics Department, Naval Postgraduate School, Monterey, CA 93943, USA

Received 2 January 2010, in final form 26 March 2010
Published 20 April 2010
Online at stacks.iop.org/SST/25/055017

Abstract
Variations in minority carrier transport properties associated with networks of misfit dislocations have been measured using a unique optical technique in p-type GaInP grown on Ge. The diffusion length L of minority carriers has been measured with a spatial resolution of 0.4 μm in regions showing alternating light and dark luminescence bands. Periodic variations of $\pm 4\%$ from a mean diffusion length of 3.9 μm were measured and found to be anti-correlated to intensity fluctuations. A model based on the coupling between luminescence intensity and minority carrier lifetime allows for the extraction of spatial variation of both radiative and non-radiative lifetimes. For this high quality material, with relatively low concentrations of non-radiative recombination centers, the results indicate variations in radiative recombination lifetime associated with dopant fluctuations.

(Some figures in this article are in colour only in the electronic version)

Introduction

The widespread use of heteroepitaxy in the semiconductor industry has led to the extensive study of the role of strain and strain relaxation in thin film growth of dissimilar materials [1, 2]. Heteroepitaxial structures are instrumental to the optimized performance of semiconductor lasers, detectors and high-efficiency solar cells. The strain that arises from lattice mismatch can be effectively utilized in thin structures, such as strained-layer lasers and high-speed transistors, to improve laser efficiency and increase device speed. Beyond a critical thickness, however, the strain is relieved through plastic deformation and the formation of misfit dislocations at the substrate–layer interface.

These dislocation patterns in lattice mismatched semiconductors have been imaged extensively via scanning photoluminescence and cathodoluminescence techniques. While their structural effects are often well characterized with transmission electron microscopy and x-ray diffraction, one of the challenges in the characterization and understanding of heteroepitaxial semiconductors is to relate these structural effects to electronic and optical properties.

In this work, we utilize a unique tool for localized characterization of minority carrier transport to study variations in minority carrier diffusion associated with misfit dislocation patterns in heteroepitaxial GaInP. By combining spatially resolved optical measurements of luminescence intensity and localized transport behavior, we are able to determine variations in both radiative and non-radiative lifetimes on a sub-micron length scale. A model is developed to quantify the correlation between intensity variations, as commonly measured in photo or cathodoluminescence, and the underlying variations in effective minority carrier lifetime and carrier diffusion that determine transport behavior.

Background

GaInP is a ternary III–V alloy that is of fundamental interest due to its tendency for spontaneous ordering and the resultant effects on bandgap, effective mass and optical anisotropy [3]. It is used extensively in solar cell applications and forms the top cell material in multi-junction solar cells that have exhibited efficiencies reaching 40% [4]. In these devices the GaInP is grown on a Ge substrate, with intermediate layers of InGaAs that form the second of the junctions for collection and

conversion of solar radiation. Although both the InGaAs and GaInP compositions are usually selected to be closely lattice matched to the Ge substrate ($In_{0.01}Ga_{0.99}As$ and $Ga_{0.51}In_{0.49}P$ respectively), a small degree of mismatch still exists and results in the formation of a relatively low concentration of misfit dislocations in layers with a thickness of $\sim 1\ \mu$m. It is the effect of this dislocation network on electronic transport properties, specifically minority carrier diffusion, that we investigate here.

Dislocations are generally found to be regions of increased non-radiative recombination for minority carriers in semiconductors, due to midgap energy levels that mediate Shockley–Read–Hall recombination. Luminescence mapping in heteroepitaxial materials often shows variations in intensity that lead to a cross hatched type pattern of bright and dark bands along the $\langle 1\,1\,0\rangle$ directions for growth on a (0 0 1) substrate [5]. The spatial variations in intensity can range from a few percent to as much as 50%, depending on the material system of interest. These intensity variations alone, however, provide no direct information about associated variations in carrier transport properties. While spatially resolved electrical characterization, such as spreading resistance or patterned device production, may yield additional insight, these measurements are often either impractical or cannot be performed with the spatial resolution of interest.

Time-resolved cathodoluminescence coupled with scanning TEM has been applied to provide the most detailed studies of recombination processes at dislocations, with much of the work focused on GaAs and GaP. Yacobi and Holt [6] review a number of studies. Although the consensus is that impurity segregation to dislocations plays an important role and that minority carrier lifetime is generally decreased in the immediate vicinity of the dislocation core, there are also conflicting results on the relationship to luminescence contrast. The model developed here sheds new light on the complex interplay of the variations on radiative and non-radiative lifetimes and the resultant intensity fluctuations.

Transport imaging is a unique approach to determining minority carrier diffusion lengths by utilizing the distribution of the recombination luminescence from localized carrier generation. It is related to but different from cathodoluminescence (CL) in that it uses an electron beam for the generation of excess carriers, but then maintains the spatial information from the recombination. In standard scanning CL, this spatial information is lost, as all luminescence resulting from excitation at a given point is assumed to be associated with that point. The benefits of transport imaging are that minority carrier diffusion lengths can be obtained directly from steady-state optical images. This has been demonstrated for determination of minority carrier drift lengths in GaAs double heterostructures under bias [7] and for determination of minority carrier diffusion lengths in materials (InGaAs, GaAs and GaP) for triple junction solar cells [8]. One benefit of the optical technique, utilized in this work, is that the spatial resolution can be higher than for many electrical techniques that measure transport properties.

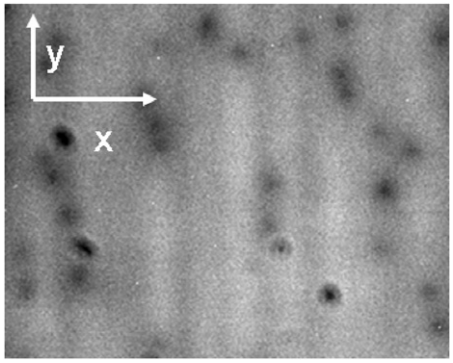

Figure 1. Cathodoluminescence imaging of 100 μm (width) $\times$ 80 μm (height) region of GaInP showing luminescence intensity variations. The incident electron beam energy is 20 keV with a probe current of 6×10^{-10} A.

Experimental approach

The sample is a double heterostructure of AlGaInP/$Ga_{0.496}$InP/AlGaInP on a (0 0 1) InGaAs/Ge substrate. The GaInP layer is 0.65 μm thick, with a 300 K bandgap (determined from PL) of 1.81 eV. The layer is p-type with a doping level of 1.1×10^{17} cm^{-3}. As previously mentioned, GaInP undergoes spontaneous CuPt ordering. The order parameter for this particular layer is estimated to be 0.43, based on empirical relationships between bandgap and degree of ordering [8]. Previously reported transport imaging measurements [8] have shown that the average minority carrier diffusion length in this sample is 3.1/3.9 μm for diffusion parallel/perpendicular to the ordering direction. This is attributed to mobility variations due to effective mass anisotropy in the ordered alloy.

The sample is placed in a JEOL scanning electron microscope. The electron beam is incident normal to the sample and generates primarily band-to-band luminescence from the sample. CL spectroscopy confirms that, because the barrier layers are thin, the luminescence signal is significant only from the GaInP layer. An optical microscope is inserted into the beam axis via a retractable arm and used to collect the luminescence, which is then imaged on a cooled 2148 $\times$ 1056 pixel CCD camera external to the SEM. The resolution of the optical image is $\sim$400 nm/pixel, determined by the $\sim$20$\times$ magnification of the optical microscope and the 6.8 μm $\times$ 6.8 μm pixel size on the CCD.

Figure 1 shows an area luminescence scan of a 100 μm $\times$ 80 μm region of the GaInP. The image was taken by exposing the region to a scanning electron beam and recording the resulting luminescence on the CCD camera. The optical effect of the dislocation network is most evident in this sample as alternating vertical bands of varying luminescence intensity.

In order to probe the effect of these material variations on the transport of minority carriers, we perform transport imaging, using the electron beam to generate a line source of excess minority carriers perpendicular to the vertical bands of varying luminescence intensity, i.e. in the x-direction on figure 1. Electron beam excitation of 20 keV was used at

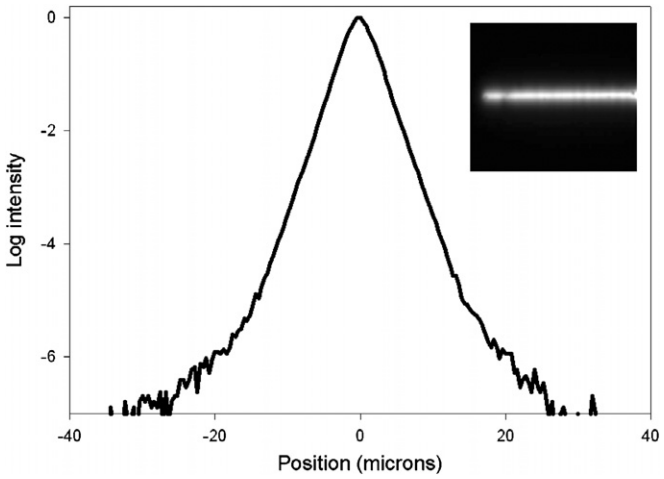

Figure 2. CCD image of the line scan excitation (inset) and extracted intensity distribution in the vertical direction.

a probe current of 6×10^{-10} A. The exposure time for the CCD image, ~20 s, is long compared to the time required to both scan the beam and to establish an equilibrium minority carrier population, resulting in a quasi-steady-state image of the luminescence distribution.

Figure 2 shows an image of the luminescence resulting from a line scan in the x-direction extending across multiple light/dark intensity bands (inset) and an example of the intensity distribution along the vertical (y) axis. The net effect of the line excitation is to produce diffusion of minority carriers in the $\pm$ y-directions within the bands. The next section describes the numerical approach to extracting minority carrier diffusion lengths from the resulting intensity distributions.

Data analysis and determination of minority carrier diffusion length

The GaInP epitaxial layer is assumed to be thin, with near zero surface recombination due to the presence of the wider bandgap barrier layers on both sides. Minority carrier concentrations therefore can be approximated as nearly constant through the thickness of the samples. The one-dimensional source is modeled by a Gaussian source distribution. With these approximations, the steady state minority carrier concentration is described by a one-dimensional diffusion problem with source and extinction terms

$$D\frac{\partial^2 u}{\partial y^2} - \frac{1}{\tau}u + \frac{G}{\sqrt{\pi\sigma}}\,\mathrm{e}^{-y^2/\sigma} = 0, \tag{1}$$

where u is the minority carrier concentration, D is the diffusivity of the minority carrier concentration, τ is the average effective lifetime of a minority carrier, and G and σ are the amplitude and variance of the line source respectively. Using standard mathematical techniques, the solution is

$$u(y) = \frac{G\tau}{4L}\left\{\mathrm{e}^{((y/L)+(\sigma/4L^2))}\left[1 - \mathrm{erf}\left(\frac{y+\sigma/2L}{\sqrt{\sigma}}\right)\right]\right.$$
$$\left. + \mathrm{e}^{(-y/L+(\sigma/4L^2))}\left[1 + \mathrm{erf}\left(\frac{y-\sigma/2L}{\sqrt{\sigma}}\right)\right]\right\}, \tag{2}$$

where $L = \sqrt{D\tau}$ is the diffusion length of the minority carriers.

We assume recombination of the electrons with a larger population of majority holes, since Δp due to the electron beam excitation is negligible compared to the existing hole concentration p, $\Delta p \ll p$. This is a good approximation for this material, with a majority carrier doping in excess of 10^{17} cm^{-3}. In this 'low injection limit' the distribution of the luminescence reflects the distribution of the minority carrier population, and therefore can be used to study diffusion behavior from a known generation source.

For this material, it has previously been experimentally determined that $L \sim 4$ μm and $\sqrt{\sigma} \sim 0.1$ μm, based on transport imaging and measurements of the incident beam diameter and sample thickness. Because $\mathrm{erf}(z) \to 1 + \frac{C}{z}\,\mathrm{e}^{-z^2}$ as $z \to \infty$, the error functions in (2) can be replaced by unity for values of y greater than 1 or 2 μm. The resulting asymptotic form for the minority carrier concentration $u(y)$ for y greater than a few microns from the line source is then

$$u(y) \approx \frac{K\tau}{L}\,\mathrm{e}^{-y/L} \quad \text{for large } y, \quad \text{where} \quad K = \frac{G}{2}\,\mathrm{e}^{\sigma/(4L^2)}. \tag{3}$$

The experimental data contain a background signal from thermal excitation in the CCD, as well as statistical noise and background illumination in the chamber, that must be removed prior to performing a least-squares fit of the data to the asymptotic form. This is done by fitting the data with a linear function at points far enough from the line source and subtracting the resulting background prior to fitting the data with the decaying exponential in equation (3).

At any given point along the line source, L is found by performing a least-squares fit to equation (3) of the minority carrier profile at a set of points emanating from the source point in a direction normal to the line source. Figure 3 shows results from two regions where we plot the maximum luminescence intensity I along the line source and the local diffusion length L extracted from the least-squares analysis. In these regions, an anti-correlation between I and L is observed, indicating that bands of decreased luminescence are associated with increased diffusion length. This anti-correlation was first reported in [9]. We present additional examples here and develop a complete data analysis and model for the behavior.

One sees from figure 3 that the CL intensity fluctuations are on the order of $\pm 9\%$. The transport imaging analysis allows for measurement of the minority carrier diffusion length to an accuracy of ~0.1 μm and also shows a $\pm 4\%$ variation from the mean in the measured value. While not all regions of the sample exhibit such clear anti-correlation between I and L, this behavior was observed at multiple locations for four different line scans. Local intensity fluctuations, associated with threading dislocations or other defects on the surface of the sample, will interfere with least-squares analysis of the intensity, which requires selection of regions that are free from these additional features.

The luminescence intensity is determined by the population of excess minority carriers, Δn, and the radiative lifetime τ_{rad} as

$$I \sim \Delta n/\tau_{\mathrm{rad}} \sim G\tau/\tau_{\mathrm{rad}} \tag{4}$$

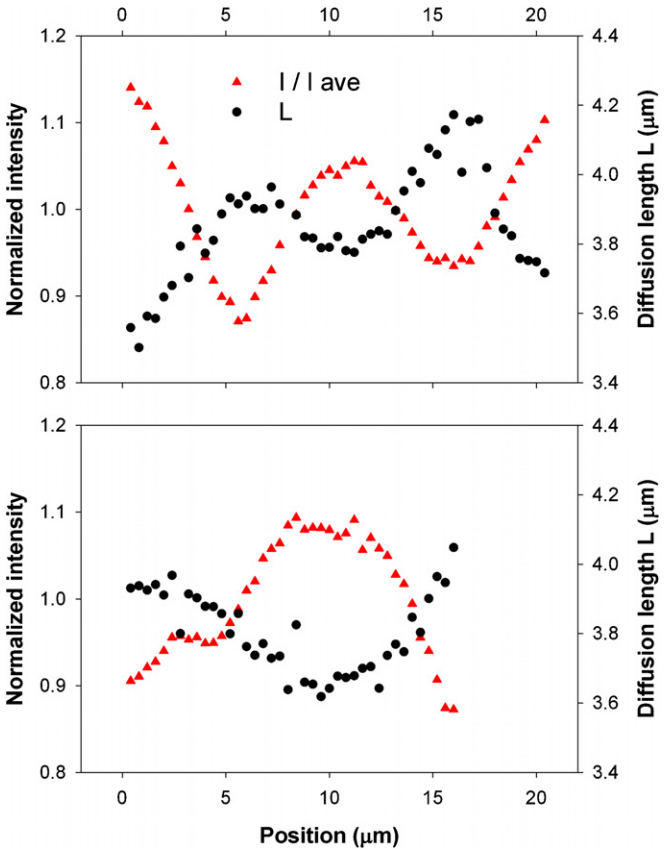

Figure 3. Two examples showing anti-correlation of intensity I (triangles) and minority carrier diffusion length L (circles) as a function of position. Average values for $L = 3.9$ μm for case 1 (upper) and 3.8 μm for case 2 (lower). Some data reproduced from figure 3 of [9].

since the steady state population of minority carriers, Δn, is itself a product of the generation rate G and the effective lifetime τ, which depends on both radiative and non-radiative recombination paths. By independently determining L, we have information on the localized variation in τ, if we assume a constant mobility in the direction of net diffusion. Based on earlier work demonstrating minority carrier lifetime fluctuations associated with dislocations [6], and the relative insensitivity of carrier mobility to low dislocation densities, we make that assumption here. We now develop a model relating intensity variations and diffusion length and thereby determine the spatial variations of both non-radiative and radiative components of the lifetime.

Mathematical model relating lifetime and intensity variations

We derive a relationship for correlations between the intensity I and the diffusion length L as a function of correlations between the non-radiative and radiative lifetimes τ_{nr} and τ_{rad}. Based on the observed fluctuations in the measured material properties, we assume that τ_{nr} and τ_{rad} are given by

$$\tau_{nr} = \tau_{nr}^{avg}[1 + \alpha\,\delta(x)], \qquad \tau_{rad} = \tau_{rad}^{avg}[1 + \beta\,\delta(x)], \tag{5}$$

where τ_{nr}^{avg}, τ_{rad}^{avg} are the spatial averages of τ_{nr} and τ_{rad}, and $\delta(x)$ is a function of position. The dimensionless numbers α and β characterize the departure of the lifetimes from their average values and are assumed to be small i.e. $\alpha, \beta \ll 1$. The function $\delta(x)$ models the variation in lifetime due to dislocations and may be approximately periodic depending on the material. The amplitudes α, β determine the effect those material variations have on the lifetimes τ_{nr} and τ_{rad}. The validity of these assumptions is borne out by comparing them with measurements for a given material. Note that when the signs of α and β are the same/opposite, the variations in the lifetimes τ_{nr} and τ_{rad} are correlated/anti-correlated.

Since

$$I \sim G(\tau/\tau_{rad}) = G(\tau_{nr}/(\tau_{rad} + \tau_{nr})) \tag{6}$$

and

$$L_d = (D\tau)^{1/2} = (D\ \tau_{nr}\tau_{rad}/(\tau_{rad} + \tau_{nr}))^{1/2}, \tag{7}$$

we can define

$$I^{avg} = G\left(\tau^{avg}/\tau_{rad}^{avg}\right) = G\left(\tau_{nr}^{avg}/\left(\tau_{rad}^{avg} + \tau_{nr}^{avg}\right)\right) \tag{8}$$

$$L^{avg} = \left(D\tau_{nr}^{avg}\tau_{rad}^{avg}/\left(\tau_{rad}^{avg} + \tau_{nr}^{avg}\right)\right)^{1/2}, \tag{9}$$

and then substitute the lifetimes τ_{nr}, τ_{rad} in (5) into I and L, and expand for small α and β. We find

$$I - I^{avg} = I^{avg}\left[\frac{\tau_{rad}^{avg}}{\tau_{rad}^{avg} + \tau_{nr}^{avg}}\right][\alpha - \beta]\delta(x) + (\text{smaller terms quadratic in } \alpha, \beta) \tag{10}$$

and

$$L - L^{avg} = \frac{L_d^{avg}}{2}\left[\frac{\alpha\tau_{rad}^{avg} + \beta\tau_{nr}^{avg}}{\tau_{rad}^{avg} + \tau_{nr}^{avg}}\right]\delta(x) + (\text{smaller terms quadratic in } \alpha, \beta). \tag{11}$$

For small α and β, the dominant contribution to the departures of I and L from their average values is given by the first term on the right side of equations (10) and (11) respectively. In these terms, the spatial variation in I and L is controlled by $\delta(x)$, and the amplitude and correlation of the departures of I and L from their average values L_d^{avg}, L^{avg} by the expressions

$$\left[\frac{\tau_{rad}^{avg}}{\tau_{rad}^{avg} + \tau_{nr}^{avg}}\right][\alpha - \beta] \quad \text{and} \quad \left[\frac{\alpha\tau_{rad}^{avg} + \beta\tau_{nr}^{avg}}{2\left(\tau_{rad}^{avg} + \tau_{nr}^{avg}\right)}\right].$$

In particular, the correlation between the departures of I and L from their average values L_d^{avg} and L^{avg} is determined by the signs of $\alpha - \beta$ and $\alpha\tau_{rad}^{avg} + \beta\tau_{nr}^{avg}$. When the signs are the same, the spatial variations in I, L are correlated; when the signs are opposite, the spatial variations in I and L are anti-correlated.

If we think of the parameters α and β as coordinates in a two-dimensional parameter plane, then the relationships determining the correlation between the lifetimes τ_{nr} and τ_{rad} given in (5) and the relationships determining the correlation between I and L given in (10) and (11) divide the parameter plane into four regions as illustrated in figure 4. Each region consists of two triangular wedges which are opposite to each

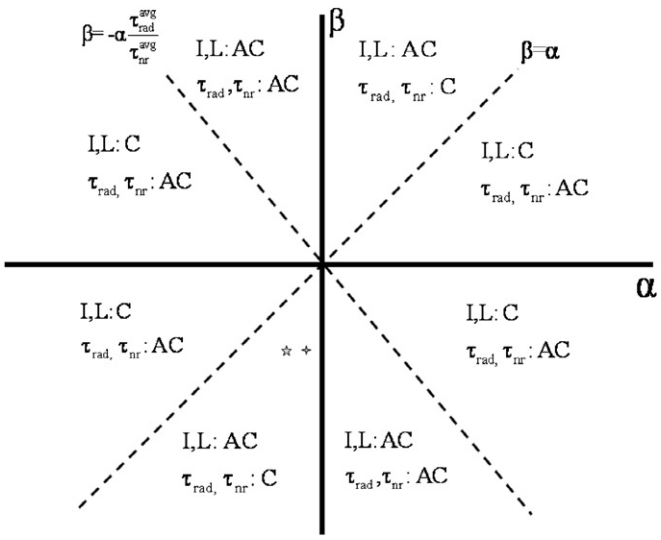

Figure 4. Schematic diagram showing the relationship between intensity (I) and diffusion length (L) dependence on variations in τ_{nr} (α) and τ_{rad} (β).

other and meet at the origin. The four regions identify parameter values for which the pairs $\tau_{nr} - \tau_{rad}$ and $I - L$ are correlated (C) or anti-correlated (AC).

Application of the model and discussion of results

Based upon the cosine series approximations, least-squares fits to both intensity and diffusion length fluctuations were independently performed. These are shown in figures 5(*a*) and (*b*), with the data and the least-squares fits normalized by their mean values. The least-squares analysis varies three parameters in producing a best fit—the mean value (constant term), the amplitude of the cosine variation and the spatial frequency of variation within the cosine function. Shifts of origins are found by inspection of the data. In each case, the fits appear to be excellent with periods of variations quite close. In particular, the relative difference in periods for I and L in each sample is about 2%. A second least-squares fit is performed on the same data which forces I and L to have the same spatial frequency parameter in their cosine series expansions. We find that all parameters in these 'combined' fits vary little from those in which I and L were fit independently, suggesting a strong spatial correlation. The scaled values of the amplitude variations are then used to determine the scaled values of the amplitude variations in τ_{rad} and τ_{nr}, i.e. β and α respectively. We obtain values of $\alpha = -0.034$ and $\beta = -0.165$ for case 1 and $\alpha = -0.029$ and $\beta = -0.165$ for case 2. These points are indicated schematically in figure 4. (Note: a change in the arbitrary selection of the phase would simply change the signs of α and β to positive values.)

Independent time resolved photoluminescence measurements provided an average τ of 13.1 ns for the sample, and an average radiative lifetime was estimated to be $\tau_{rad} \sim 37.7$ ns from $\tau_{rad} = 1/(Bp)$, where p is the average majority carrier doping and B is the recombination coefficient [10, 11]. Figures 6(*a*) and (*b*) plot the resulting variations

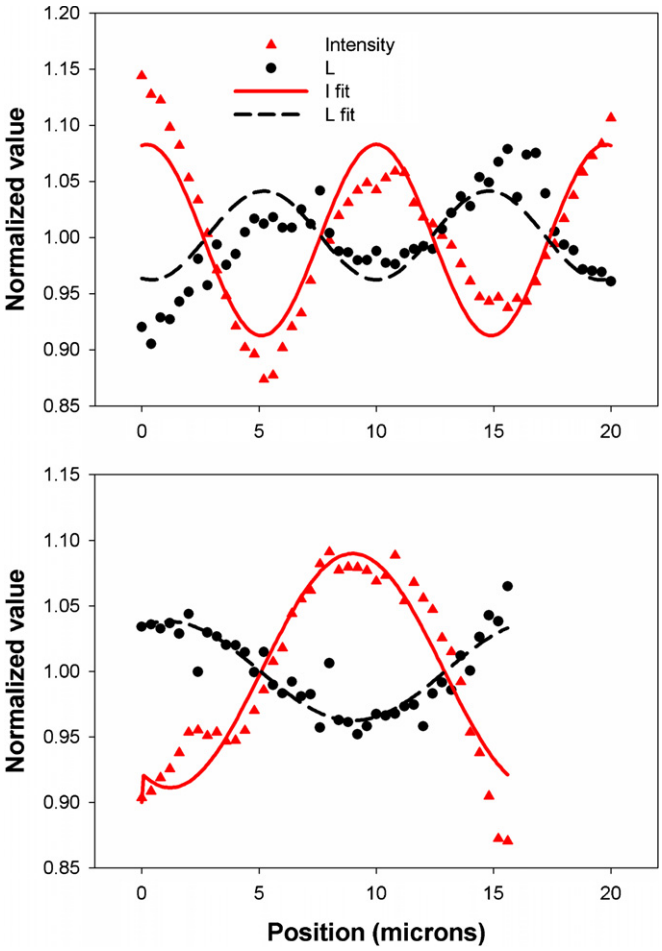

Figure 5. Least-squares fits to the intensity and diffusion length data. Results are normalized to the average value to indicate percent variations.

in τ_{rad}, τ_{nr}, and τ along the line source derived from the variations in I and L for cases 1 and 2 respectively.

This analysis shows how an increase in luminescence intensity can occur in a region where a decreased τ must cause a decreased minority carrier diffusion length. For the case demonstrated here, where α and β have the same sign, the requirement is a variation in radiative lifetime, where the amplitude of that variation is larger than the variation in non-radiative lifetime. Such a variation can occur if the dislocations result in spatial variations in the net majority carrier population. This could result either from variations in the primary dopant concentration associated with local strain relief or in the resulting hole population due to compensating defects. Our results indicate that the brighter regions are associated with a shorter radiative lifetime, and therefore a larger free hole population. If one assumes that the shorter minority carrier lifetime occurs in the vicinity of the dislocation core, then this suggests that, in this material, a larger free hole population occurs in this same region, which both decreases the radiative lifetime ($\tau_{rad} \sim 1/p$) and increases the intensity. Thus the luminescence is stronger near the dislocations, even though the minority carrier lifetime is shorter.

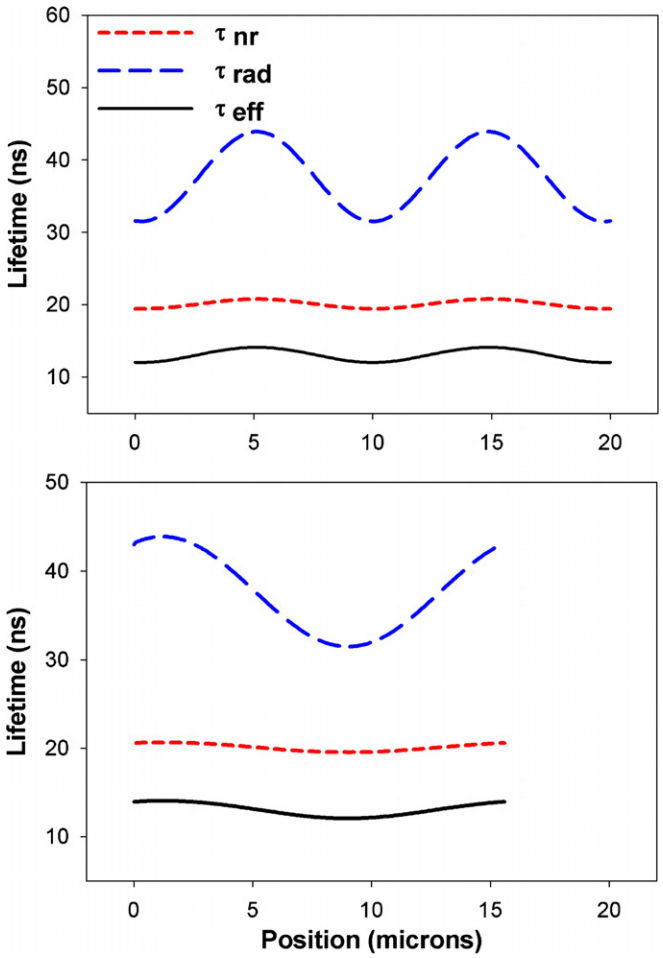

Figure 6. Resulting spatial variations in radiative, non-radiative and effective lifetimes. The value $B = 2.4 \times 10^{-10}$ cm^3 s^{-1} for InGaP was used for calculation of the average radiative lifetime.

This non-intuitive result arises from the fact that, in these high quality materials, the non-radiative and radiative lifetimes are comparable, with a relatively low concentration of defects leading to non-radiative recombination and relatively small fluctuations (2–3%) in τ_{nr}. In materials where larger fluctuations in τ_{nr} are dominant ($\alpha > \beta$), one sees from figure 4 that I and L will always be correlated—i.e. regions of shorter effective lifetime and lower diffusion length are regions of lower intensity. We have demonstrated here, however, that in high quality materials with variations in τ_{rad}, the opposite behavior is possible. The possibility of either result—correlation or anti-correlation between I and L depending on actual material properties—may explain the wide variations of reports in the literature that attempt to correlate optical and electronic parameters near dislocations.

In summary, we have used optical imaging of carrier transport to measure variations in minority carrier diffusion length associated with the network of misfit dislocations in a heteroepitaxial sample of GaInP. Variations in minority carrier diffusion length were measured with a spatial resolution of 0.4 μm and found, in certain regions of the sample, to be anti-correlated to intensity fluctuations associated with misfit dislocations. A model based on the coupling between luminescence intensity and minority carrier lifetime allows for the extraction of spatial variation of both radiative and non-radiative lifetimes. For this high quality material, with relatively low concentrations of non-radiative recombination centers, the results support models of dopant and/or compensating defect fluctuations related to dislocations, resulting in periodic and measurable variations in minority carrier transport properties.

Acknowledgments

This work was supported by the National Science Foundation under grant no DMR-0526330 and by the DNDO Academic Research Initiative under grant no ARI/NSF 083007. The GaInP heterostructure material was grown by C Fetzer of Spectrolab Inc. We acknowledge helpful discussions with H J Yoon and R King of Spectrolab Inc.

References

[1] Dunstan D J 1997 *J. Mater. Sci., Mater. Electron.* **8** 337
[2] Beanland R, Dunstan D J and Goodhew P J 1996 *Adv. Phys.* **45** 87
[3] Mascarenhas A 2002 *Spontaneous Ordering in Semiconductor Alloys* (New York: Kluwer)
[4] King R R *et al* 2007 *Appl. Phys. Lett.* **90** 183516
[5] Petroff P M, Logan R A and Savage A 1980 *Phys. Rev. Lett.* **44** 287
[6] Yacobi B G and Holt D B 1990 *Cathodoluminescence Microscopy of Inorganic Solids* (New York: Plenum) p 179
[7] Luber D R, Bradley F M, Haegel N M, Talmadge M C, Coleman M P and Boone T D 2006 *Appl. Phys. Lett.* **88** 163509
[8] Haegel N M, Mills T J, Talmadge M, Scandrett C, Frenzen C, Yoon H, Fetzer C M and King R R 2009 *J. Appl. Phys.* **105** 023711
[9] Haegel N M, Williams S E, Frenzen C and Scandrett C 2009 *Physica* B **404** 4963–6
[10] King R R *et al* 2002 *Proc. of the 29th Photovoltaics Specialists Conf. (IEEE, New York, 2002)* pp 776–81
[11] Strauss U, Ruehle W W and Queisser H J 1994 *J. Appl. Phys.* **75** 8204